Published online 29 October 2009 *Nucleic Acids Research, 2010, Vol. 38, No. 1* **203–214**
doi:10.1093/nar/gkp904

The RNA polymerase activity of SARS-coronavirus nsp12 is primer dependent

Aartjan J. W. te Velthuis[1], Jamie J. Arnold[2], Craig E. Cameron[2], Sjoerd H. E. van den Worm[1] and Eric J. Snijder[1,*]

Molecular Virology Laboratory, Department of Medical Microbiology, Center of Infectious Diseases, Leiden University Medical Center, PO Box 9600, 2300RC Leiden, The Netherlands and [2]Department of Biochemistry and Molecular Biology, Pennsylvania State University, University Park, Pennsylvania 16802, USA

Received September 15, 2009; Revised October 5, 2009; Accepted October 6, 2009

ABSTRACT

An RNA-dependent RNA polymerase (RdRp) is the central catalytic subunit of the RNA-synthesizing machinery of all positive-strand RNA viruses. Usually, RdRp domains are readily identifiable by comparative sequence analysis, but biochemical confirmation and characterization can be hampered by intrinsic protein properties and technical complications. It is presumed that replication and transcription of the ~30-kb severe acute respiratory syndrome (SARS) coronavirus (SARS-CoV) RNA genome are catalyzed by an RdRp domain in the C-terminal part of nonstructural protein 12 (nsp12), one of 16 replicase subunits. However, thus far full-length nsp12 has proven refractory to expression in bacterial systems, which has hindered both the biochemical characterization of coronavirus RNA synthesis and RdRp-targeted antiviral drug design. Here, we describe a combined strategy involving bacterial expression of an nsp12 fusion protein and its *in vivo* cleavage to generate and purify stable SARS-CoV nsp12 (106 kDa) with a natural N-terminus and C-terminal hexahistidine tag. This recombinant protein possesses robust *in vitro* RdRp activity, as well as a significant DNA-dependent activity that may facilitate future inhibitor studies. The SARS-CoV nsp12 is primer dependent on both homo- and heteropolymeric templates, supporting the likeliness of a close enzymatic collaboration with the intriguing RNA primase activity that was recently proposed for coronavirus nsp8.

INTRODUCTION

The central enzymatic activity in the life cycle of positive-strand RNA (+RNA) viruses is the process of RNA-templated RNA synthesis. In mammalian cells, the replication of +RNA genomes always occurs in the cytoplasm where the viral RNA-synthesizing machinery is commonly associated with (modified) cytoplasmic membranes, which presumably provide physical support and may serve to protect the complex from host defense mechanisms (1,2). The viral enzyme complex contains an RNA-dependent RNA polymerase (RdRp) as its core catalytic subunit for the production of negative strand RNA (–RNA), new genome molecules and in many virus groups also subgenomic (sg) messenger RNAs (mRNAs) (1,3).

Coronaviruses (CoVs) are a family of +RNA viruses that infect a wide range of vertebrates including humans, as exemplified by severe acute respiratory syndrome (SARS) and various respiratory infections caused by less-virulent family members (4). The group is also known for its exceptionally large polycistronic genome of ~30 kb, which is 5′ capped and 3′ polyadenylated RNA. The 5′-proximal two-thirds of the CoV genome (open reading frames 1a and 1b) are translated into the viral replicase polyproteins pp1a and pp1ab. The 3′-proximal third encodes the viral structural proteins and several so-called accessory proteins, which can only be expressed following the production of a set of four to nine sg mRNAs (5,6). In particular, it is this CoV hallmark that has attracted attention over the years, since these sg mRNAs consist of sequences that are noncontiguous in the viral genome: a common 5′ leader sequence is attached to body segments representing a variable part of the 3′-proximal genomic region. According to the now widely supported transcription model of Sawicki and Sawicki (7), the arterivirus and CoV sg RNAs derive from a discontinuous step during minus-strand RNA synthesis that is guided by specific RNA signals and resembles copy-choice RNA recombination (5,6,8). This mechanism produces a set of subgenome-length negative-strand templates from which the sg mRNAs are produced. The unusual genome size of CoVs and the complexity of their RNA synthesis hint at

*To whom correspondence should be addressed. Tel: +31 71 5261657; Fax: +31 71 5266761; Email: e.j.snijder@lumc.nl

an RdRp that may have special properties, either by itself or in conjunction with other subunits of the CoV replication/transcription complex (RTC).

CoV replication and transcription are driven by the 15 or 16 viral nonstructural proteins (nsps) encoded in the replicase gene, which include many enzyme activities that are rare or lacking in other families of +RNA viruses (9,10). These nsps are produced during co- and post-translational processing of the pp1a and pp1ab replicase polyproteins by two or three internal viral proteinases (11). In the years following the 2003 SARS outbreak, bioinformatics, structural biology, (reverse) genetics and biochemical studies have all contributed to the in-depth characterization of CoV nsps in general and those of SARS-CoV in particular (9,10,12). Currently documented enzyme activities include proteinases (11), a putative RNA primase (13), a superfamily 1 helicase (14), an exo- and an endoribonuclease (15,16), single-stranded RNA (ssRNA)-binding proteins (17,18) and two methyltransferases (19,20). Following the sequence analysis of the first CoV genomes, more than two decades ago, the putative RdRp domain of the coronavirus RTC had already been identified by comparative sequence analysis (21,22). The C-terminal, two-thirds of the 932-amino-acid subunit, now known as nsp12 was confidently aligned with the conserved motifs of well-known RdRps (22,23). In view of its unprecedented size among viral RdRp subunits, which commonly consist of 500–600 amino acids, nsp12 may well harbor other functional domains in its as-yet uncharacterized N-terminal domain. Biochemical information on the CoV RdRp has, however, remained scarce thus far, particularly since full-length nsp12 was refractory to expression in bacterial systems. Preliminary evidence for the *in vitro* RdRp activity of nsp12 came from a study of the SARS-CoV enzyme by Cheng *et al*. (24). However, their experiments, employing a glutathione S-transferase (GST)-nsp12 fusion protein, were hampered by protein instability, which resulted in the fragmentation of the protein into three parts. Primer-dependent activity on poly(A) templates was observed in filter binding assays, but the enzyme biochemistry was not further characterized in detail.

Given its pivotal role in viral replication and the efficacy of polymerase inhibitors used to combat other virus infections, the SARS-CoV RdRp is widely regarded as an important and attractive target for the rational design of anti-CoV drugs (23,25). We therefore sought to solve the technical issues described above and develop reliable protocols for stable expression, purification and *in vitro* activity of the full-length CoV nsp12. In this article, we describe an expression strategy utilizing *in vivo* cleavage in a bacterial expression system by ubiquitin carboxyl-terminal hydrolase 1 (Ubp1), which releases the small N-terminal fusion partner ubiquitin (Ub) and generates a recombinant nsp12 protein containing its natural N-terminus. This was found to be a critical step on the road toward purification of a stable recombinant SARS-CoV RdRp. We subsequently established that full-length nsp12 can readily synthesize RNA in a primer-dependent fashion on both homo- and heteropolymeric RNA templates and is also efficient at incorporating deoxy-nucleotides on a DNA template. This work therefore provides a solid basis for the further biochemical characterization of the coronavirus nsp12 and the detailed dissection of its role in viral replication and transcription. Understanding the enzyme's properties will be essential for the development of selective coronavirus RdRp inhibitors and will likely provide novel insights into the intriguing (evolutionary) relation between the RdRp of nidoviruses and other groups of +RNA viruses.

MATERIALS AND METHODS

Cloning and expression of recombinant SARS-CoV nsp12

The amino acid sequence of SARS-CoV nsp12, residues S4370 to Q5301 of replicase pp1ab, is fully conserved among all sequenced SARS-CoV isolates. For our study, the nsp12-coding region was amplified by reverse transcription-polymerase chain reaction (RT-PCR) from the genome of SARS-CoV Frankfurt-1 (AY291315). During amplification, the ORF1a/1b −1 ribosomal frameshift near the 5′-end of the gene was corrected in a translationally silent manner. Primers used for amplification were SAV424 5′-GCGGGTACCCCGCGGTGGATCTGCGGATGCATCAA-3′ and SAV425 5′-GCGCGATCGGGATCCCTGCAAGACTGTATGT-3′, corresponding to SARS-CoV genome positions 13 327–13 387 and 16 152–16 166, respectively. The PCR amplicon was digested with SacII and BamHI, and ligated into expression vector pET26-Ub-CHis$_6$ (26). Following confirmation of the nucleotide sequence of the amplicon and using the flanking XbaI and XhoI restriction sites, the ubiquitin-nsp12-His$_6$ fusion gene (Ub-nsp12-CHis$_6$) was subcloned into vector pASK3 (IBA) and thereby placed under the control of a tetracycline-inducible promoter. This ruled out the known risk of potential contamination with T7 RNA polymerase, as it can occur when using a T7 promoter to drive expression of other RdRps in bacterial expression systems. Nsp12 active-site mutant D618A, carrying an Asp618Ala substitution, was engineered via site-directed mutagenesis according to the QuikChange protocol (Stratagene), using primers SAV526 5′-CCTTATGGGTTGGGCTTATCCAAAATGTG-3′ and SAV527 5′-CACATTTTGGATAAGCCCAACCCATAAGGA-3′.

For nsp12 expression, the pASK3-Ub-nsp12-CHis$_6$ plasmid was transformed to *Escherichia coli* C2523 cells (New England Biolabs) together with the Ubp1 protease expression plasmid pCGI (26), unless indicated otherwise for particular experiments. Routinely, 250 ml of Luria Broth, containing ampicillin (50 μg/ml) and chloramphenicol (34 μg/ml), was inoculated 1:1000 with 3 ml o/n precultures and cells were grown at 37°C to OD$_{600}$ >0.7. Subsequently, the cells were slowly cooled to room temperature, tetracycline was added to a final concentration of 200 μg/ml and the cells were further grown at 20°C for another 16 h. Cells were harvested by centrifugation, washed once with ice-cold phosphate-buffered saline (PBS) and stored at −20°C until protein purification.

SARS-CoV nsp12 expression vectors pKM596-nsp12 (kindly provided by Dr. Isabelle Imbert and Dr. Bruno Canard) and pET102-Thio-nsp12 (a kind gift of

Dr. Susanne Pfefferle and Dr. Christian Drosten) were used to transform *E. coli* BL21(DE3) cells and expression was performed using the auto-induction medium ZYM-5052 (27).

Purification of SARS-CoV nsp12-His

Cell pellets were thawed on ice, resuspended in binding buffer (20 mM HEPES pH 7.4, 500 mM NaCl, 20 mM imidazole, 10% glycerol, 0.05% Tween-20 and 5 mM β-mercaptoethanol) and lysed by sonication. Cell debris was removed by ultra-centrifugation at 20 000 *g* and the cleared supernatant was incubated with Talon beads (Clontech) for 2 h at 4°C. The beads were washed three times with 20 vol of binding buffer, loaded onto spin columns and finally the His-tagged protein was eluted with 300 mM imidazole in binding buffer. The eluate was analyzed by sodium dodecyl sulfate polyacrylamide gel electrophoresis (SDS–PAGE) and typically found to be 80–85% pure. Subsequently, gel filtration on a Superdex 200 column (GE Healthcare) in 20 mM HEPES, 500 mM NaCl, 5% glycerol, 5 mM β-mercaptoethanol and 0.1% Tween-20 was used to improve purity to ~95%. To estimate the molecular mass of nsp12, a standard curve for hydrodynamic elution was made using chymotrypsinagen A, conalbumin, aldolase and dextran blue (all purchased from GE Healthcare) as size markers and fitted to a linear equation ($R^2 = 0.99$).

After the gel filtration step, the nsp12-containing fractions were pooled, concentrated with Ultrafree 10-kDa filter columns (Millipore) and dialyzed overnight against 1000 sample volumes of dialysis buffer (20 mM HEPES pH 7.4, 100 mM NaCl, 0.1% Triton-X 100, 1 mM DTT and 50% glycerol) in cellulose tubing (SnakeSkin, Pierce). Protein concentrations were determined using a Bradford assay and a bovine serum albumin (BSA) standard curve, and the purified protein was stored at −20°C. When using expression vectors pKM596-nsp12 and pET102-Thio-nsp12, protein purification procedures were essentially similar to those described above, except that amylose resin (New England Biolabs) was used to bind the pMK596-nsp12 product, which was eluted using a buffer containing 10 mM amylose instead of imidazole.

SDS–PAGE and western blotting

Cells were lysed in Laemmli's sample buffer (28), separated on 8% SDS–PAGE gels and either electroblotted to polyvinylidene fluoride (PVDF) membrane (GE Healthcare) or stained directly with Coomassie G-250 according to standard protocols. Prior to incubation with a SARS-CoV nsp12-specific rabbit antiserum (a kind gift from Dr. Mark Denison) (29), blot membranes were blocked with 10% skimmed milk and 0.02% Tween-20 in PBS. Blots were washed with 0.02% Tween-20 in PBS, incubated with a swine-anti-rabbit horseradish peroxidase conjugate diluted in 5% skimmed milk, 0.02% Tween-20 and PBS, washed and subjected to ECL Plus chemiluminescence detection (GE Healthcare).

Preparation of templates

RNA oligonucleotides and their DNA counterparts SAV557R 5′ -GCUAUGUGAGAUUAAGUUAU-3′ and SAV481R 5′-UUUUUUUUUUAUAACUUAAUC UCACAUAGC-3′, SAV555R 5′- UUUUUUUUUUU UUUUUUUUUAUAACUUAAUCUCACAUAGC-3′ and SAV556R 5′-UCUCUCUCUCUCUCUCUCUCAU AACUUAAUCUCACAUAGC-3′ were purchased from Eurogentec, excised as a single band from 7 M urea/15% polyacrylamide gels, eluted overnight in deionized water and desalted using NAP-10 columns (GE Healthcare). To anneal RNA duplexes, oligonucleotide mixtures in annealing buffer [20 mM Tris–HCl pH 8.0, 50 mM NaCl and 5 mM ethylenediaminetetraacetic acid (EDTA)] were heat denatured, slowly cooled to room temperature and subsequently purified from 15% nondenaturing polyacrylamide gels.

RdRp activity assays

To test the *in vitro* RdRp activity of SARS-CoV nsp12-CHis$_6$, 0.1 μM of the protein (unless otherwise indicated) was incubated at 30°C in the presence of 1 μM template, 0.17 μM [α-^{32}P]ATP (0.5 μCi/μl; Perkin-Elmer), 50 μM ATP (Roche), 20 mM Tris–HCl (pH 8.0), 10 mM NaCl, 10 mM KCl, 6 mM $MgCl_2$, 5% glycerol, 0.01% Triton-X 100, 1 mM DTT and 0.5 U of RNaseOUT (Invitrogen). Glycerol and NaCl were introduced with the addition of enzyme due to their presence in the nsp12 storage buffer. RdRp reactions were terminated by adding an equal volume of 90% formamide, 50 mM EDTA pH 8.0, 0.01% bromophenol blue and xylene cyanol. Reaction products were analyzed on 7 M Urea, 20% polyacrylamide gels buffered with 1× TBE (90 mM Tris, 90 mM H_3BO_3 and 2 mM EDTA). Gels were run for 5 h at 2000 V and analyzed using phosphorimaging. Plates were scanned on a Typhoon variable mode scanner (GE Healthcare) and products were quantified with ImageQuant TL 7.0 (GE Healthcare). To calculate the amount of [α-^{32}P]AMP incorporated from the phosphorimager signal, a 10^{-2}–10^{-5} dilution series of the [α-^{32}P]ATP stock was spotted in triplicate on Whatman filter and exposed alongside the PAGE gel of interest. Using the standard curve, phosphorimager counts were converted into the amount of label incorporation and kinetic traces were fit to a linear function with the MATLAB 2008b Curve Fitting Toolbox (Mathworks).

Electrophoretic mobility shift assays

A dilution series of SARS-CoV RdRp in storage buffer was incubated for 10 min at room temperature with 0.2 nM of ^{32}P-labeled oligonucleotide SAV557R (see above), in the presence or absence of the complementary oligonucleotide SAV481R. Samples were then directly loaded on to 8% acrylamide gels containing 5% glycerol and 0.5× TBE and were run at 100 V for 2 h at 4°C. Gels were dried on Whatman filter paper and bands were quantified by phosphorimaging. Using the MATLAB 2008b Curve Fitting Toolbox, the percentage of RNA

bound was fit to the Hill equation $RNA_{bound} = b*[nsp12]^n/(K_d^n + [nsp12]^n)$, where b is the upper binding limit, [nsp12] is the nsp12 concentration, n is the Hill coefficient and K_d is the enzyme's dissociation constant.

RESULTS

Stable expression and purification of full-length SARS-CoV nsp12

A PCR amplicon encoding SARS-CoV nsp12 was first cloned into T7 expression vector pET26-Ub-CHis$_6$, which provided the 932-aa viral protein with an N-terminal Ub tag (76 amino acids) and a C-terminal hexahistidine tag (Figure 1A). To avoid the known risk of T7 RNA polymerase contamination when purifying another RdRp using a T7 promoter-driven expression system [like *E. coli* BL21(DE3)], the Ub-nsp12-CHis$_6$ fusion gene was subsequently transferred to plasmid pASK3, placing it under control of a tetracycline-inducible promoter. Initially, the protease that was later used to remove the Ub tag was not co-expressed and the expression of the full-length Ub-tagged nsp12-CHis$_6$ was compared to that of variants containing either maltose binding protein (MBP) or thioredoxin (Thio) as fusion partner. As shown in Figure 1B and as also documented in the previous work of Cheng *et al.* (24), expression and purification of nsp12 fusion proteins resulted in the abundant and progressive fragmentation of the protein. Based on their sizes in SDS–PAGE, the cleavage products likely were the 64- and 39-kDa nsp12 degradation products as found by Cheng *et al.* (24) when working with their GST-nsp12 fusion construct (Figure 1B). Therefore, our results confirmed and extended the previously reported observations regarding the instability of SARS-CoV nsp12 when expressed in *E. coli* as part of a fusion protein.

In studies with the poliovirus (PV) RdRp (3D^{pol}), it was previously shown that N-terminal foreign sequences, even the addition of a single methionine residue, can have a significant impact on enzyme activity (26,30). Structural studies subsequently revealed that a native N-terminus is required for the proper folding of the RdRp's 'fingers' subdomain and the positioning of the 3D^{pol} active

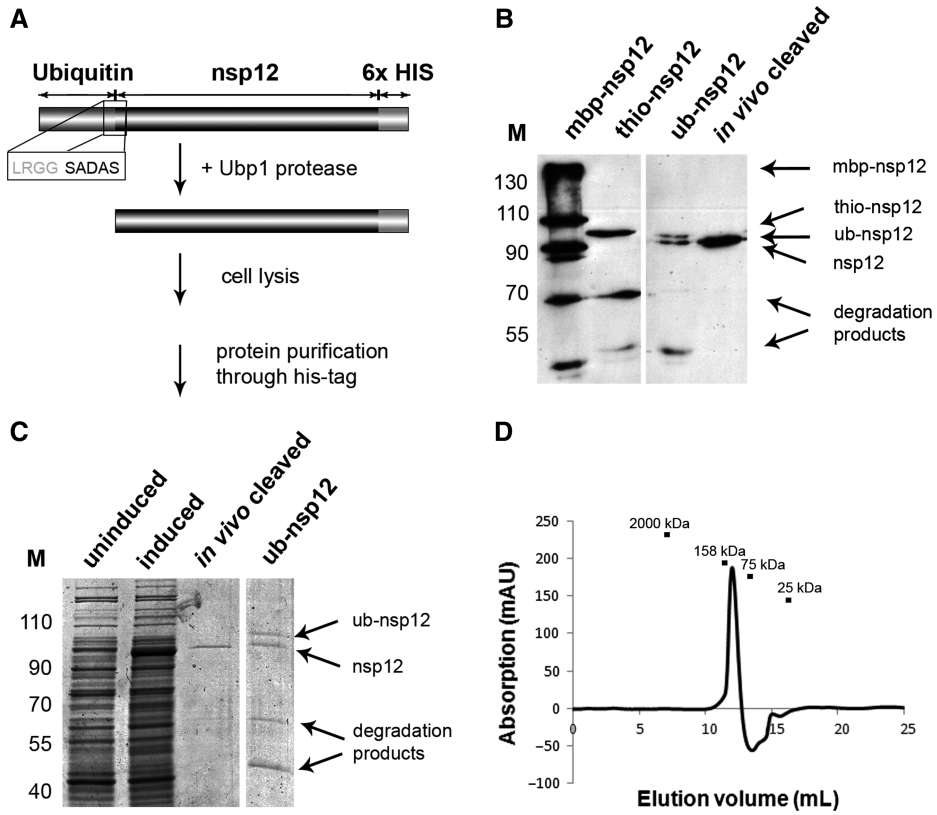

Figure 1. Expression and purification of the SARS-CoV nsp12. (**A**) Expression of nsp12 was performed in the presence of the ubiquitin (Ub) protease Ubp1, which removed the N-terminal Ub fusion partner by cleaving after the LRGG signature that formed the junction between the Ub and nsp12 moieties. This *in vivo* cleavage created the native nsp12 amino-terminus with the sequence SADAS. (**B**) Western blotting using an nsp12-specific polyclonal antiserum identified a single band of the expected mass after purification of the *in vivo* cleaved expression product. Isolation of fusion proteins with different N-terminal tags resulted in common patterns of degradation. Similar results were reported by Cheng *et al.* (24) for a GST-nsp12 fusion protein. (**C**) Purified nsp12-CHis$_6$ was readily visualized by Coomassie staining as a ~106-kDa protein product, in line with the expected mass. Inductions in the absence of Ubp1 expression, however, resulted in a mixture of full-length fusion protein and degradation products, likely as a result of improper folding. No RdRp activity was observed for these preparations. (**D**) Gel filtration analysis of purified nsp12 in assay buffer showed a single peak, corresponding to a globular molecular weight of 140 ± 10 kDa, suggesting that only the monomeric form of nsp12 is present under the conditions used.

site (30). These findings suggested to us that N-terminal additions might also hamper the proper folding of the SARS-CoV RdRp and could thus be the principal cause of its subsequent degradation. We therefore co-expressed the C-terminal Ub protease Ubp1 (26), which specifically recognizes the cleavage site in our fusion protein that is located between the Ub moiety and the N-terminus of nsp12 (*LRGG*↓SADAS). Proteolytic cleavage of the fusion protein at this site liberated an nsp12-$CHis_6$ product (Figure 1A), now containing its natural N-terminus. The expression of the Ubp1 protease was driven by the relatively weak constitutive ADH1 promoter (26). Hence, to ensure optimal release of nsp12-$CHis_6$ by the protease, induction of Ub-nsp12-$CHis_6$ expression was performed only in the middle or late log-phase of bacterial growth. Induction at lower densities or on-column cleavages performed with the cleavable MBP and Thio fusion proteins resulted in significant amounts of degraded nsp12, which was inactive in RdRp assays (data not shown).

As depicted in Figure 1B and C, the *in vivo* cleavage product that we were able to routinely purify was of the expected 106-kDa size (9) and was found to be stable, even after multiple rounds of purification and prolonged storage at −20°C. Non-denaturing gel filtration yielded a single peak corresponding to a size of about 140 ± 10 kDa as estimated by comparison to a standard curve (Figure 1E–F). This is different from the calculated mass of 106 kDa, but may be explained by, e.g. a very open or nonglobular structure of the protein. Moreover, unexpected behavior in gel filtration is not without precedent for RdRps, as was, e.g. reported for the monomeric φ6 RdRp P2 (31). Future structural studies involving electron microscopy or crystallography will hopefully allow us to address this question in more detail.

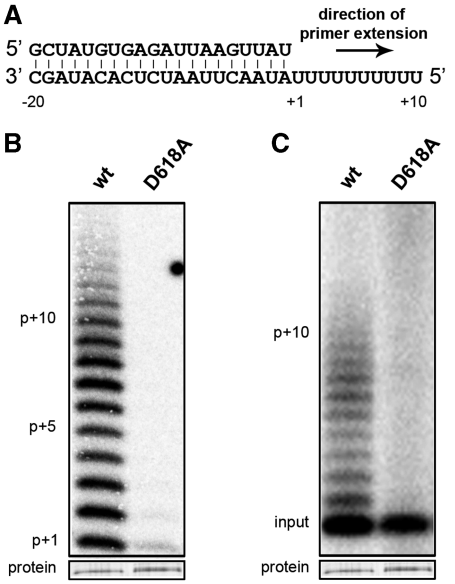

Figure 2. SARS-CoV nsp12 primer extension assay and active-site mutant. (**A**) Schematic showing the structure of the partially double-stranded RNA template with 3′ U_{10} stretch that served as template for primer extension in the initial nsp12-based nucleotide incorporation assay. (**B**) Comparison of the RdRp activity of wild-type nsp12 and a D618A active-site mutant, which displayed minimal activity after a 60-min incubation at 30°C. (**C**) A primer extension assay using a 5′ ^{32}P-labeled primer and ATP confirmed that wild-type nsp12, in contrast to the D618A mutant, was able to elongate the 20-mer primer. The slight reduction of input primer in the D618A lane probably resulted from degradation by RNase activity. The D618A mutant showed 8 ± 3% residual activity (mean of three independent experiments). In the loading control (Figure 2B and C, lower panels) the two nsp12 variants were visualized by silver staining of an SDS–PAGE gel.

SARS-CoV nsp12 is a primer-dependent RdRp

+RNA virus replication may proceed through a variety of scenarios, but essentially viral RdRps employ only two fundamentally different mechanisms during the first step of RNA synthesis: initiation can occur either *de novo*, when the 3′ hydroxyl group of the first nucleotide essentially is the 'primer' to which a second nucleotide is added, or initiation can depend on an oligonucleotide or protein primer (32). Imbert *et al.* (13) recently showed that the CoV nsp8 subunit, a relatively small protein (22 kDa) that forms a hexadecameric complex with nsp7 (33), can synthesize short oligonucleotides using poly(C) templates or templates containing a 3′ CCG/U motif. Although the exact role of nsp8 remains to be studied in much more detail, one of its proposed functions is that of an 'RNA primase' (13). According to this hypothesis, and similar to what has been documented for cellular DNA polymerases (34), the oligonucleotide products of nsp8 activity would serve as primers for the viral 'main RdRp', i.e. nsp12. Some other observations were also consistent with the possibility that the SARS-CoV main RdRp belongs to the class of primer-dependent polymerases. First, modeling of the structure of SARS-CoV nsp12 residues 400–900 suggested that the central domain of the protein contains a G motif, a signature present in all primer-dependent RdRps (23). Second, when using the unstable GST-nsp12 fusion protein in combination with a poly(A) template and a poly(U) primer, Cheng *et al.* (24) observed a moderate RdRp activity in filter-binding assays. Convincing evidence for the extension of an RNA primer *in vitro*, however, has not been documented thus far.

To qualitatively assess the polymerase activity of the nsp12, we monitored the incorporation of nucleotides on a well-defined synthetic RNA template, which was predicted to lack secondary structures that could affect the enzyme's processivity. This template (Figure 2A) consisted of a 20-nt duplex and a 3′ overhang of 10 uridylates, which could serve as template during extension of the 20-mer primer. As shown in Figure 2, primer extension was revealed by both the incorporation of [α-^{32}P]ATP (Figure 2B) and the extension of the ^{32}P-labeled primer (Figure 2C). The use of single-stranded or homopolymeric [poly(U) or poly(C)] templates did not lead to significant incorporation of nucleotides (data not shown).

Based on sequence alignments of SARS-CoV nsp12 with RdRps of known structure, it was previously concluded that the canonical aspartic acid residues responsible for the coordination of the divalent cation in the RdRp's active site should be nsp12 residues 618, 760

and 761, the latter two amino acids being part of the nidovirus-specific SDD motif (23,35–37). In other viral RdRps, single or multiple substitutions of the equivalent residues with alanine or asparagine were shown to change or even abolish polymerase activity (38,39), depending on the assay conditions used. For the PV $3D^{pol}$, for example, it was found that mutagenesis of the motif C core sequence, changing it from GDD to GDN, was detrimental in the presence of Mg^{2+}, but not when Mn^{2+} or Fe^{2+} were provided as divalent cation (38). To obtain an active site mutant that could be used as negative control during further development of our assays, we engineered nsp12 mutant D618A. As portrayed in Figure 2B and C, the mutant protein displayed only 8 ± 3% residual primer extension activity in our assays (Figure 2B–D), thus confirming the nsp12-specific nature of the RdRp activity described here and supporting the prior hypothesis that this residue is a key player in the enzyme's active site. Further or complete knockdown of activity may be obtained under slightly different assay conditions or in combination with substitution of other active site residues, which remain to be tested in future studies.

Biochemical determinants of the *in vitro* activity of the SARS-CoV nsp12

It is common practice to employ filter binding assays during optimization of polymerase activity assays. Although convenient and less time consuming than gel analysis of reaction products, these assays merely reveal incorporation of label, but do not provide direct information on the length and integrity of the products. Therefore, when exploring the effects of different reaction buffer compositions, we consistently quantified and analyzed [α-^{32}P]ATP incorporation using denaturing 20% acrylamide gels. The standard assay buffer consisted of 20 mM Tris–HCl (pH 8.0), 10 mM KCl, 1 mM DTT, 6 mM $MgCl_2$, 5% glycerol, 0.1% Triton-X 100 and 50 μM ATP.

First, the influence of reaction temperature on RdRp activity was tested within the range of 20–37°C. Activity at 37°C was 40% higher than at 30°C, which is more commonly used in RdRp assays (Figure 3A) (37,40–42). However, a more detailed analysis revealed that this increase largely stemmed from enhanced initiation of primer extension rather than elongation, with the latter being decreased by 35% as judged from the amount of full-length product (primer + 10, Figure 3B). Therefore, all subsequent experiments were performed at 30°C. Contrary to expectations however, the major extension product never matched the length of the primer plus 10 nt, suggesting that nsp12 generally terminates before reaching the end of the primed poly(U) template. The results obtained with other templates are discussed subsequently.

It is well established that nucleic acid polymerases utilize divalent cations, mostly Mg^{2+}, as cofactors to bind and coordinate the incoming nucleotide during the polymerization reaction (35,36). As shown in Figure 3C and D, the activity of nsp12 was positively correlated with the Mg^{2+} concentration and reached its optimum at 6 mM. Higher concentrations (≥20 mM) ultimately abolished activity (data not shown). The SARS-CoV RdRp does not require Mn^{2+} for RNA synthesis, as previously reported for the nsp9-RdRp of the arterivirus equine arteritis virus (EAV), a distant relative in the order *Nidovirales* (37). In fact, the presence of Mn^{2+} in an RdRp assay utilizing a poly(U) template decreased the fidelity of the SARS-CoV nsp12 relative to Mg^{2+} and facilitated both transversional and transitional misincorporations (Figure 4). The specificity for the nucleotide's sugar moiety seemed not affected, however, since deoxyadenosine triphosphate (dATP) was not incorporated when using an RNA template in the presence of Mn^{2+}. This discriminates the SARS-CoV RdRp from, e.g. its PV equivalent, for which correct base pairing was more important than the presence of a 2′ hydroxyl group (40).

To establish the importance of pH, we tested SARS-CoV RdRp activity in the pH range of 6.0–8.5. We clearly observed an increase of nsp12 overall activity with an optimum at pH 8.0 (Figure 3E), but differences between pH 7.0 and 8.5 were marginal in terms of both overall activity and amount of full-length product produced (Figure 3F). Interestingly, pH 7.5 consistently resulted in a significantly larger amount of initiation product, suggesting that higher pH values stimulate the processivity of the enzyme.

In additional assays, we tested the effect of monovalent cations, bovine serum albumin and spermidine (data not shown). No negative influence of potassium or sodium ions was observed below a concentration of 50 mM. Neutral to slightly negative effects were found for both BSA (tested for 0–0.1 mg/ml), which is known to stabilize enzymes and reduce potential side effects such as absorbance to the plastic surface of the reaction tube used. Finally, addition of spermidine, which binds to the phosphate backbone of nucleic acids and is a known stimulator of various polymerases, did not improve activity in the tested concentration range up to 5 mM.

RNA-binding properties of SARS-CoV nsp12

Our combined observations suggested that nsp12 is only active in a primer-dependent fashion and may thus prefer binding to double-stranded RNA (dsRNA). To determine the affinity of nsp12 for dsRNA and ssRNA we performed electrophoretic mobility shift assays, in which we titrated purified nsp12 in the presence of 0.2 nM 5′-^{32}P-labeled RNA (Figure 5). Subsequently, the percentage of bound template and the Hill equation (see 'Materials and Methods' section) were used to derive the enzyme's dissociation constants (K_d). For dsRNA the K_d was calculated at 0.13 ± 0.03 μM, whereas the K_d for ssRNA was estimated to be 0.10 ± 0.02 μM.

Nsp12 nucleotide incorporation rates

For various viral RdRps, *in vitro* studies have defined biochemical properties that could not be determined or were largely obscured in *in vivo* assays. Furthermore, following the basic characterization of individual enzymes, the interplay with templates, cofactors and other subunits of the

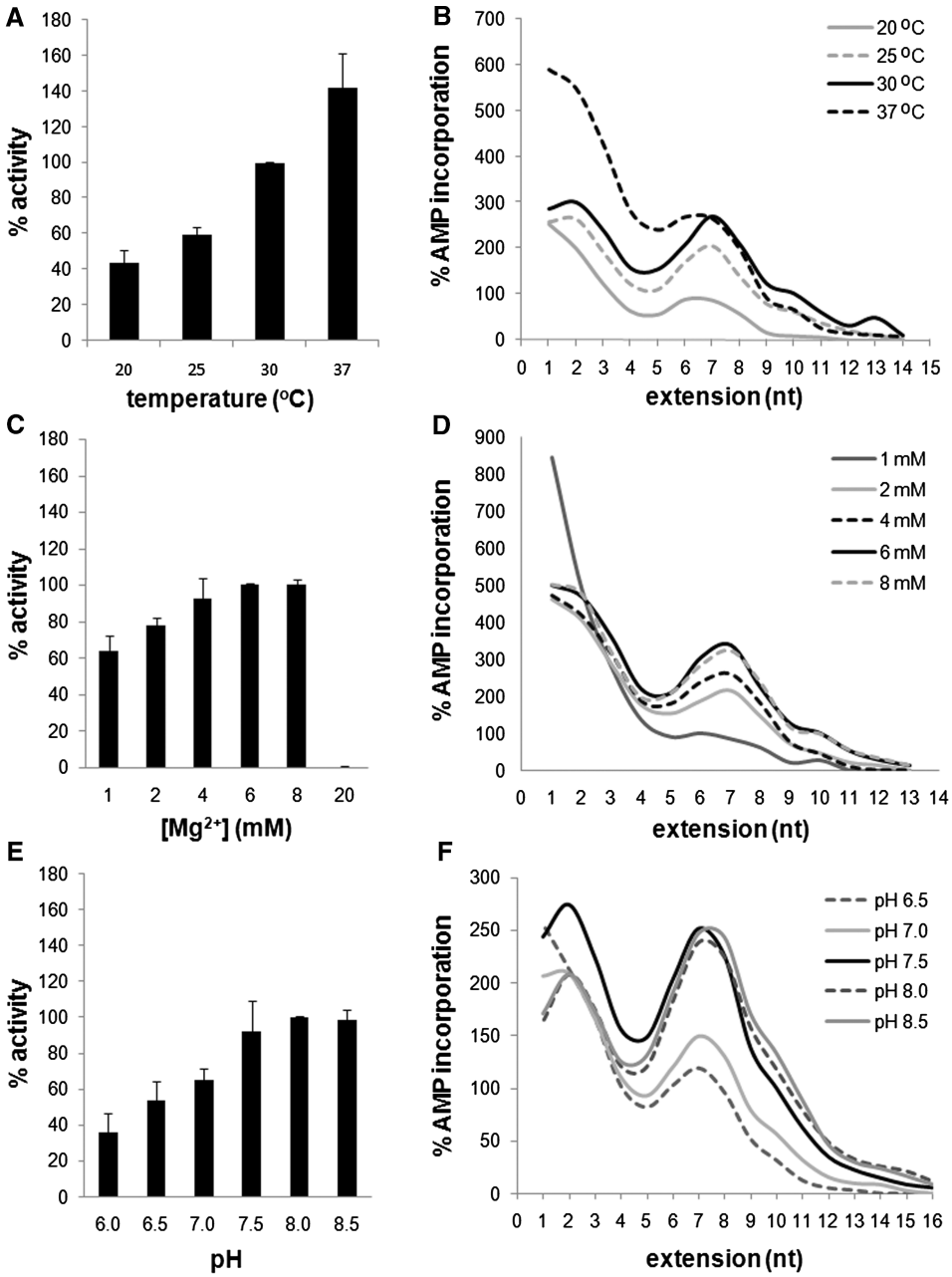

Figure 3. Biochemical determinants of SARS-CoV nsp12 activity. (**A** and **B**) Tests to determine the influence of temperature indicated that nsp12 incorporates ATP most efficiently at 37°C, although this effect mainly stemmed from increased initiation. Based on these results, 30°C was taken as the standard for subsequent experiments. (**C** and **D**) Titration of the Mg^{2+} concentration showed that activity reaches its maximum at 6 mM. (**E** and **F**) The effect of pH on RdRp activity was evident as well, with lower pHs limiting the activity of the enzyme. All reactions were incubated for 60 min at 30°C, unless otherwise indicated. Error bars in A, C and E represent standard error of the mean ($n = 3$).

viral enzyme complex can be addressed. Ultimately, this should facilitate the *in vitro* reconstitution of the holoenzyme complex and the analysis of its interactions at each step of viral replication and transcription. After the purification of active SARS-CoV nsp12 and exploration of the reaction conditions, our subsequent step toward such a future goal was to evaluate the rate of nucleotide incorporation by the SARS-CoV RdRp. On a primed U_{10} template we found relatively poor incorporation rates (1.2 ± 0.4 nM/min) and a major product that was 2–3 nt shorter than the expected full-length product (Figure 6A), with product sizes displaying a similar Gaussian-like distribution as depicted in the graphs in Figure 3. On the other hand, we also observed minor products that were slightly longer than full length, suggesting slippage of the polymerase at the end of the template. We did not detect any terminal transferase activity on the templates used (data not shown).

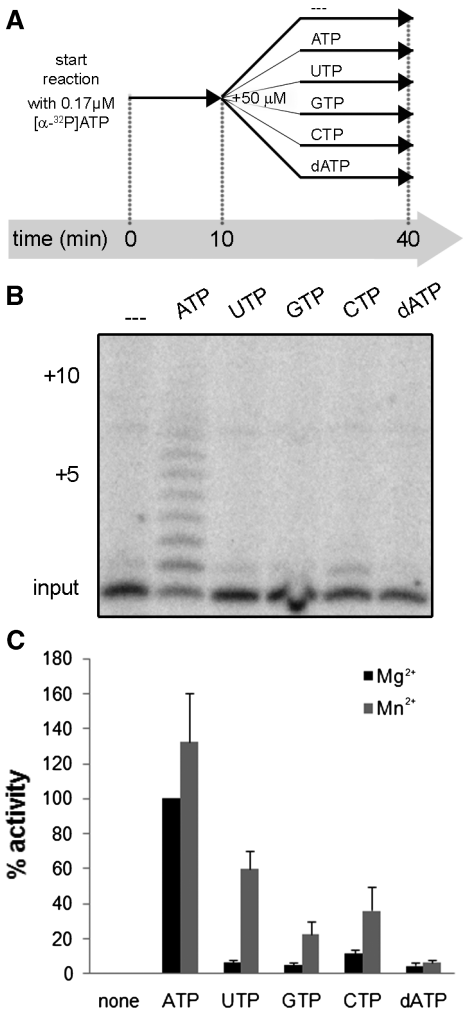

Figure 4. Nucleotide incorporation fidelity of nsp12. (**A**) Experimental set-up of pulse-chase experiments with different nucleotides and a primed poly(U) template (see Figure 2A). The reactions were initiated with a limiting concentration of [α-^{32}P]ATP to allow the incorporation of a first nucleotide and the formation of a stable polymerase-template complex. Subsequently, after 10 min, different unlabeled nucleotides were added to a final concentration of 50 μM to allow elongation for another 30 min. (**B**) SARS-CoV nsp12 allows only limited transversional and transitional misincorporations. Interestingly, also in the presence of dATP no significant activity was observed, implying that the SARS-CoV RdRp is capable of discriminating between ATP and dATP. (**C**) Pulse-chase experiments in the presence of 6 mM Mn^{2+} show that manganese ions promote misincorporation of ribonucleotides (both transversions and transitions). The selection against dATP remained unaltered.

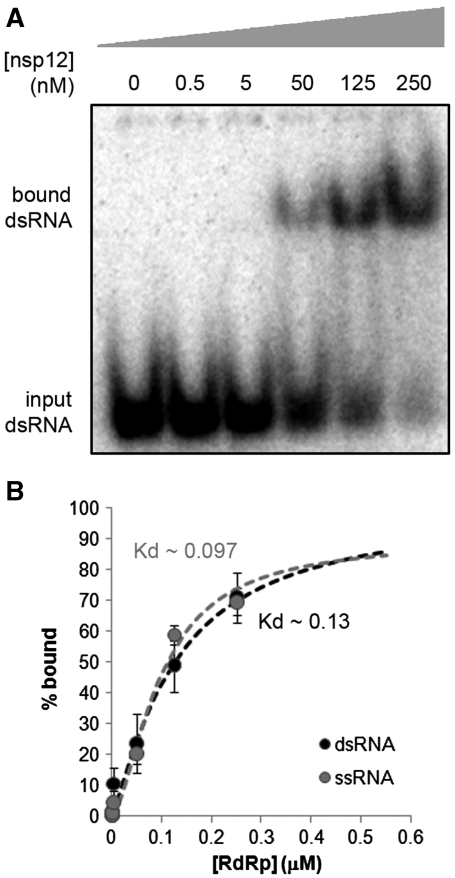

Figure 5. RNA binding affinity of nsp12. (**A**) A fixed concentration (0.2 nM) of radiolabeled dsRNA or ssRNA (data not shown) was titrated with purified nsp12 and the complexes formed were separated from unbound RNA on a native 8% polyacrylamide gel. (**B**) Free and bound RNA were quantified and fit to the Hill equation (see 'Materials and Methods' section), resulting in K_d values of 0.13 ± 0.3 μM for dsRNA and 0.10 ± 0.2 μM for ssRNA binding. R^2 values of these Hill fits were 0.97 and 0.98 for dsRNA and ssRNA, respectively. Error bars represent standard error of the mean (n = 3).

Previously, Cheng *et al.* (24) reported that their unstable GST-nsp12 fusion protein had limited reverse transcriptase activity. In contrast to these prior results, our nsp12 was not able to efficiently use dATP to extend an RNA primer (Figure 4A and B) and a similar result was obtained with a DNA primer (data not shown). To test whether nsp12 was able to incorporate [α-^{32}P] deoxyadenosine monophosphate (dAMP) when using DNA templates, we employed a primed T_{10} template similar to the RNA templates described above. As shown in Figure 6B, nsp12 was capable of incorporating dAMP when incubated with a DNA template. On average, a minor reduction (~20%) in dAMP incorporation was observed in comparison to the activity on an RNA template. The size distribution of products was more different, and showed significantly less initiation than on an RNA template (compare Figure 6A and B).

The incorporation rate of nsp12 increased dramatically when we doubled the template length (V_{U20} = 27 ± 3 nM/min, Figures 6C and 7), but we again observed a major product that was 2 nt shorter than the expected full-length product. When the primed poly(U) template was changed to a primed heteromeric $(CU)_{10}$, nsp12 activity increased further ($V_{(CU)10}$ = 45 ± 2 nM/min) and reached a level comparable to that obtained for other viral RdRps on similar short templates (40). When the products of the latter reactions were resolved by denaturing PAGE (Figure 6D) they were found to be longer than template length. Similar products extending beyond unit length have been often observed when short templates were

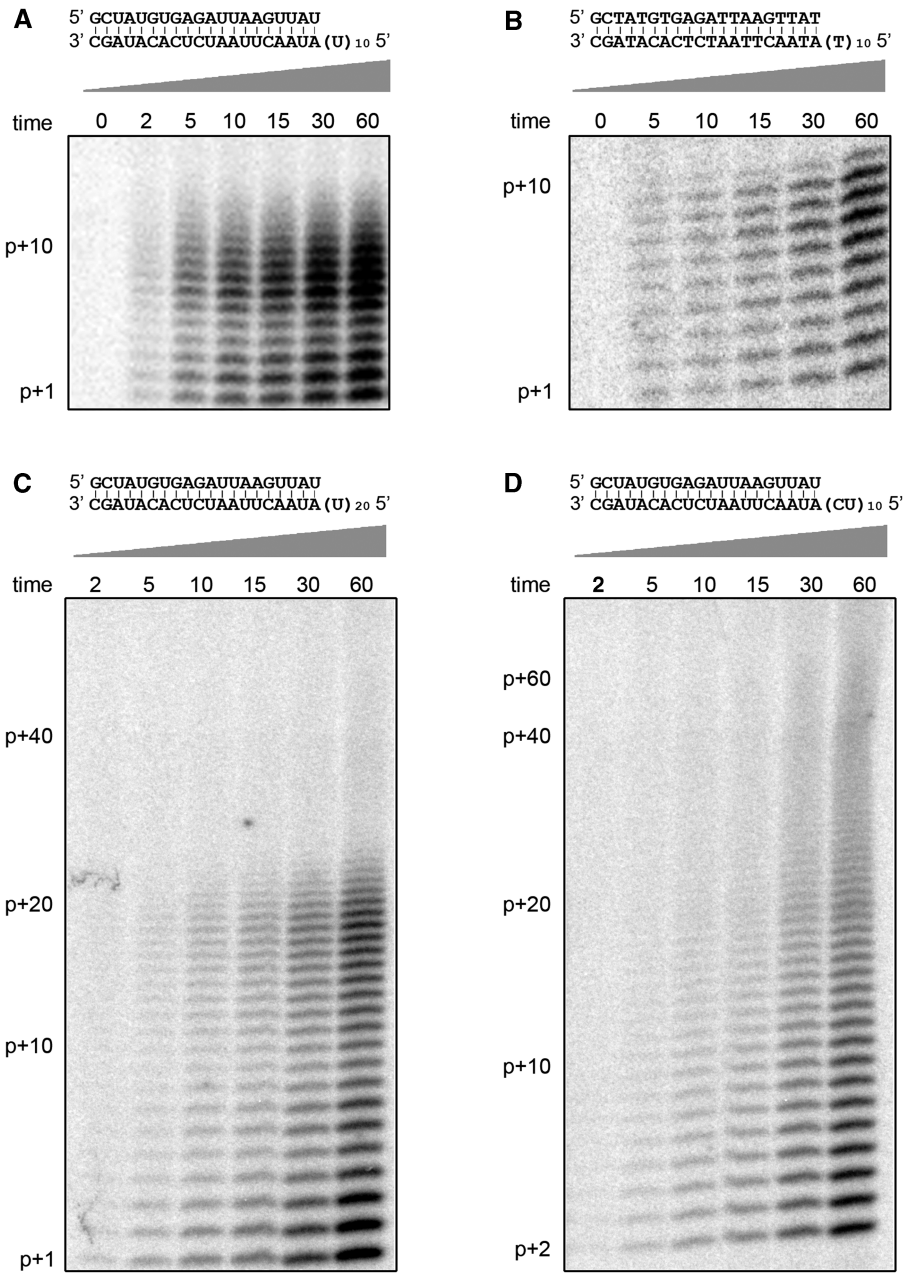

Figure 6. Analysis of nucleotide incorporation by nsp12. (**A**) Reactions with 0.1 μM nsp12, 1 μM template and 50 μM ATP were followed over time and quenched with 50 mM EDTA at the time points indicated. Gel analysis showed that, similar to the curves in Figure 3, the major accumulating product is the primer (p) extended by 7 nt (i.e. p + 7) and not the expected full-length product of n + 10. (**B**) To assess whether nsp12 was capable of DNA-templated incorporation of dATP, reactions were performed as in Figure 6A, but now using a DNA template. The time course illustrates robust [α-^{32}P]dAMP incorporation, implying that the SARS-CoV RdRp is able to utilize both RNA and DNA templates. The incorporation of dAMP was 20% lower than that of AMP on an RNA template. (**C**) Time courses were additionally performed using an RNA template containing a U_{20} template region. Similar to the shorter 10-nt template used in Figure 6A, the major product here was around 2 nt shorter than the expected full-length product. (**D**) Changing the single-stranded template from U_{20} to a heteromeric $(CU)_{10}$ not only increased the nucleotide incorporation rate by 34%, but also the behavior of nsp12 on the template. Products of the expected full-length size (p + 20) were observed, but also products longer than the template, hinting at, e.g. template switching by nsp12. Future research will address this observation in more detail. In this reaction both 50 μM ATP and GTP were present. The gel image represents the top half of a 20% denaturing PAGE gel.

used for PV 3D^{pol} (43) and their generation can be explained by various mechanisms, such as distributive slippage, processive slippage, template switching or terminal transferase activity (43 and references therein). Future research is expected to address these mechanisms in more detail.

DISCUSSION

Detailed kinetic and stoichiometric information plays an important role in explaining the molecular basis of RdRp-catalyzed ribonucleotide incorporation, the associated mutation rate of viral genomes and, consequently, RNA

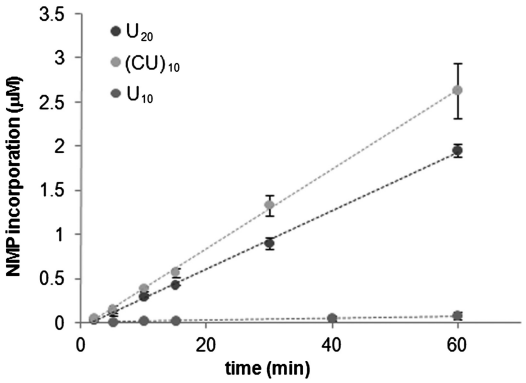

Figure 7. Analysis of the nucleotide incorporation rate of nsp12. Steady-state time courses were performed with 0.1 μM nsp12 as described in Figure 6. Experimental data were subsequently fit to linear regression to obtain NMP incorporation rates. These clearly illustrated an increase of the incorporation velocity with template length ($V_{U10} = 1.2 \pm 0.4$ nM/min and $V_{U20} = 27 \pm 3$ nM/min) and from homopolymeric template to copolymeric template ($V_{(CU)10} = 45 \pm 2$ nM/min). R^2 values were 0.97, 0.99 and 0.99, respectively, and error bars indicate standard error of the mean ($n = 3$).

virus evolution. Furthermore, a comprehensive understanding of the differences between viral RdRps and cellular polymerases is crucial in the design of specific inhibitors of viral RNA synthesis and their subsequent mechanistic characterization and optimization. Up till now, all of the above information was particularly limited, if not completely lacking, for the CoV RdRp, due to enzyme insolubility, instability and low purification yields.

This study reports the first successful expression and purification of stable, soluble SARS-CoV nsp12, thus paving the way for its further biochemical characterization. Using a two-step procedure, the protein was purified to near homogeneity, as confirmed by SDS–PAGE and non-denaturing gel filtration. We found that even a single-step purification scheme could produce an enzyme preparation that combined specific activity with reasonable purity (>80–85%). Of particular importance in our expression protocol was the co-expression of the Ubp1 protease that mediated the *in vivo* removal of the N-terminal Ub tag (Figure 1A) (26). Apparently, similar to PV $3D^{pol}$ (30), SARS-CoV RdRp does not tolerate additional amino acids at its N-terminus, likely because they induce an unstable and largely inactive fold. Because of the observed sensitivity to N-terminal fusions, it is tempting to speculate that the processing of the pp1ab cleavage generating the nsp12 N-terminus is of great importance for proper folding and activity *in vivo* as well. In line with this notion, it was reported that for the related group 2 CoV mouse hepatitis virus (MHV) this cleavage site indeed is indispensable for virus replication (44). It still remains to be tested whether there is any effect of the C-terminal His-tag on the activity of the enzyme used in this study.

The SARS-CoV nsp12 is a relatively large protein (932-amino-acid residues), e.g. much larger than the well described RdRps of HCV (591 amino acids) and PV (461 amino acids), and may have, in addition to the C-terminal RdRp domain, other functional or contributing domains in its still uncharacterized N-terminal domain(s). Previously, the PV and HCV RdRps were demonstrated to bind RNA with K_d values of 2–10 μM (45) and ~3 μM (46), respectively. Our data suggest that SARS-CoV nsp12 binds RNA with slightly higher affinity for both dsRNA and ssRNA ($K_d \sim 0.1$ μM). The relatively similar affinities for dsRNA and ssRNA suggest that the lack of *de novo* initiation may largely be due to a relatively open structure and the absence of a conserved priming loop in the predicted thumb subdomain (23). The latter structural element, a β-hairpin in, e.g. hepatitis C virus (HCV) NS5B, is present in many known *de novo* initiating RNA polymerases. Canonically, it functions by partly obstructing the template binding cleft and is believed to be essential for association with the single-stranded 3′ end of the template RNA (23,47,48).

Contrary to previous GST-pull downs performed for nsp12 (49) and data obtained for other RdRps such as the PV $3D^{pol}$—which was reported to form multimers and even lattices (45)—we were not able to establish nsp12 multimerization using non-denaturing gel filtration. Although this suggests that SARS-CoV RdRp exists predominantly as monomer under the conditions used here, it is likely that nsp12 binds to various other viral replicase subunits (50) and cellular cofactors (51) *in vivo*. The CoV holo-enzyme complex formed in this manner may have more finely tuned characteristics than documented in this study. In addition, it remains to be tested whether the C-terminal hexahistidine tag interferes with multimerization. Clearly, these and other questions should be addressed in more detail in future studies.

Upon binding to template and primer, we found nsp12 to have reproducible nucleotide incorporation rates on the templates tested, but incorporation depended significantly on the length of the template. Furthermore, on heteromeric templates the SARS-CoV RdRp also performed better and reached incorporation rates in the same order (>nM/min) as the model polymerases from PV and HCV, when correcting for enzyme and template concentrations (40,52). In addition, the SARS-CoV nsp12 is also active on a DNA template, which may greatly facilitate further investigations in view of the superior stability of DNA templates and the fact that various other SARS-CoV enzymes (17,33,53) have documented affinity for DNA as well. It remains to be tested whether SARS-CoV nsp12 is also active on a longer single-stranded template, e.g. RNA templates based on the terminal sequences of the viral genome, and whether it is able to traverse the RNA secondary structures present in such a molecule. Taken together, our data suggest that our present purification scheme and assay constitute a concrete starting point for further biochemical exploration of the SARS-CoV RdRp and nsp12 targeted inhibitor development.

ACKNOWLEDGEMENTS

The authors acknowledge Dr. Alexander Gorbalenya, Dr. Mark Denison, Dr. Nynke Dekker, Steve Cramer,

Dr. Susanne Pfefferle, Dr. Christian Drosten, Dr. Isabelle Imbert and Dr. Bruno Canard for helpful discussions or providing reagents.

FUNDING

Funding for open access charge: The Netherlands Organization for Scientific Research (NWO; Top talent grant 021.001.037); the Council for Chemical Sciences (NWO-CW; ECHO grant 700.55.002); and by grant AI45818 from NIAID/NIH (to J.A. and C.C.).

Conflict of interest statement. None declared.

REFERENCES

1. Ahlquist,P., Noueiry,A.O., Lee,W.-M., Kushner,D.B. and Dye,B.T. (2003) Host factors in positive-strand RNA virus genome replication. *J. Virol.*, **77**, 8181–8186.
2. Salonen,A., Ahola,T. and Kaariainen,L. (2005) Viral RNA replication in association with cellular membranes. *Curr. Top. Microbiol. Immunol.*, **285**, 139–173.
3. Miller,W.A. and Koev,G. (2000) Synthesis of subgenomic RNAs by positive-strand RNA viruses. *Virology*, **273**, 1–8.
4. Perlman,S. and Netland,J. (2009) Coronaviruses post-SARS: update on replication and pathogenesis. *Nat. Rev. Micro.*, **7**, 439–450.
5. Pasternak,A.O., Spaan,W.J. and Snijder,E.J. (2006) Nidovirus transcription: how to make sense? *J. Gen. Virol.*, **80**, 1403–1421.
6. Sawicki,S.G., Sawicki,D.L. and Siddell,S.G. (2007) A Contemporary view of Coronavirus transcription. *J. Virol.*, **81**, 20–29.
7. Sawicki,S.G. and Sawicki,D.L. (1995) Coronaviruses use discontinuous extension for synthesis of subgenome-length negative strands. *Adv. Exp. Med. Biol.*, **380**, 499–506.
8. van Marle,G., Dobbe,J.C., Gultyaev,A.P., Luytjes,W., Spaan,W.J.M. and Snijder,E.J. (1999) Arterivirus discontinuous mRNA transcription is guided by base pairing between sense and antisense transcription-regulating sequences. *Proc. Natl Acad. Sci. USA*, **96**, 12056–12061.
9. Snijder,E.J., Bredenbeek,P.J., Dobbe,J.C., Thiel,V., Ziebuhr,J., Poon,L.L., Guan,Y., Rozanov,M., Spaan,W.J. and Gorbalenya,A.E. (2003) Unique and conserved features of genome and proteome of SARS-coronavirus, an early split-off from the coronavirus group 2 lineage. *J. Mol. Biol.*, **331**, 991–1004.
10. Gorbalenya,A.E., Enjuanes,L., Ziebuhr,J. and Snijder,E.J. (2006) Nidovirales: evolving the largest RNA virus genome. *Virus Res.*, **117**, 17–37.
11. Ziebuhr,J., Snijder,E.J. and Gorbalenya,A.E. (2000) Virus-encoded proteinases and proteolytic processing in the Nidovirales. *J. Gen. Virol.*, **81**, 853–879.
12. Bartlam,M., Yang,H. and Rao,Z. (2006) Structural insights into SARS coronavirus proteins. *Curr. Opin. Struct. Biol.*, **15**, 664–672.
13. Imbert,I., Guillemot,J., Bourhis,J., Bussetta,C., Coutard,B., Egloff,M., Ferron,F., Gorbalenya,A. and Canard,B. (2006) A second, non-canonical RNA-dependent RNA polymerase in SARS Coronavirus. *EMBO J.*, **25**, 4933–4942.
14. Seybert,A., Hegyi,A., Sidell,S. and Ziebuhr,J. (2000) The human coronavirus 229E superfamily 1 helicase has RNA and DNA duplex-unwinding activities with 5′-to-3′ polarity. *RNA*, **6**, 1056–1068.
15. Minskaia,E., Hertzig,T., Gorbalenya,A.E., Campanacci,V., Cambillau,C., Canard,B. and Ziebuhr,J. (2006) Discovery of an RNA virus 3′ to 5′ exoribonuclease that is critically involved in coronavirus RNA synthesis. *Proc. Natl Acad. Sci. USA*, **103**, 5108–5113.
16. Ivanov,K.A., Hertzig,T., Rozanov,M., Bayer,S., Thiel,V., Gorbalenya,A.E. and Ziebuhr,J. (2004) Major genetic marker of nidoviruses encodes a replicative endoribonuclease. *Proc. Natl Acad. Sci. USA*, **101**, 12694–12699.
17. Egloff,M.P., Ferron,F., Campanacci,V., Longhi,S., Rancurel,C., Dutartre,H., Snijder,E.J., Gorbalenya,A.E., Cambillau,C. and Canard,B. (2004) The severe acute respiratory syndrome-coronavirus replicative protein nsp9 is a single-stranded RNA-binding subunit unique in the RNA virus world. *Proc. Natl Acad. Sci. USA*, **101**, 3792–3796.
18. Su,D., Lou,Z., Sun,F., Zhai,Y., Yang,H., Zhang,R., Joachimiak,A., Zhang,X.C., Bartlam,M. and Rao,Z. (2006) Dodecamer structure of severe acute respiratory syndrome Coronavirus nonstructural protein nsp10. *J. Virol.*, **80**, 7902–7908.
19. Decroly,E., Imbert,I., Coutard,B., Bouvet,M., Selisko,B., Alvarez,K., Gorbalenya,A.E., Snijder,E.J. and Canard,B. (2008) Coronavirus Nonstructural protein 16 is a Cap-0 binding enzyme possessing (nucleoside-2'O)-methyltransferase activity. *J. Virol.*, **82**, 8071–8084.
20. Chen,Y., Cai,H., Pan,J.a., Xiang,N., Tien,P., Ahola,T. and Guo,D. (2009) Functional screen reveals SARS coronavirus nonstructural protein nsp14 as a novel cap N7 methyltransferase. *Proc. Natl Acad. Sci. USA*, **106**, 3484–3489.
21. Boursnell,M.E.G., Brown,T.D., Foulds,I.J., Green,P.F., Tomley,F.M. and Binns,M.M. (1987) Completion of the sequence of the genome of the coronavirus avian infectious bronchitis virus. *J. Gen. Virol.*, **68**, 57–77.
22. Gorbalenya,A.E., Koonin,E.V., Donchenko,A.P. and Blinov,V.M. (1989) Coronavirus genome: prediction of putative functional domain in the non-structural polyprotein by comparitive amino acid sequence analysis. *Nucleic Acids Res.*, **17**, 4847–4861.
23. Xu,X., Liu,Y., Weiss,S., Arnold,E., Sarafianos,S.G. and Ding,J. (2003) Molecular model of SARS coronavirus polymerase: implications for biochemical functions and drug design. *Nucleic Acids Res.*, **31**, 7117–7130.
24. Cheng,A., Zhang,W., Xie,Y., Jiang,W., Arnold,E., Sarafianos,S.G. and Ding,J. (2005) Expression, purification, and characterization of SARS coronavirus RNA polymerase. *Virology*, **335**, 165–176.
25. De Clercq,E. (2004) Antivirals and antiviral strategies. *Nat. Rev. Microbiol.*, **2**, 704–720.
26. Gohara,D., Ha,C., Kumar,S., Ghosh,B., Arnold,J., Wisniewski,T. and Cameron,C. (1999) Production of "authentic" poliovirus RNA-dependent RNA polymerase (3D(pol)) by ubiquitin-protease-mediated cleavage in Escherichia coli. *Protein Expr. Purif.*, **17**, 128–138.
27. Studier,F. (2005) Protein production by auto-induction in high density shaking cultures. *Protein Expr. Purif.*, **41**, 207–234.
28. Laemmli,U. (1970) Cleavage of structural proteins during the assembly of the head of bacteriophage T4. *Nature*, **227**, 680–685.
29. Prentice,E., McAuliffe,J., Lu,X., Subbarao,K. and Denison,M.R. (2004) Identification and characterization of severe acute respiratory syndrome coronavirus replicase proteins. *J. Virol.*, **78**, 9977–9986.
30. Thompson,A.A. and Peersen,O.B. (2004) Structural basis for proteolysis-dependent activation of the poliovirus RNA-dependent RNA polymerase. *EMBO J.*, **23**, 3462–3471.
31. Makeyev,E.V. and Bamford,D.H. (2000) Replicase activity of purified recombinant protein P2 of double-stranded RNA bacteriophage phi6. *EMBO J.*, **19**, 124–133.
32. van Dijk,A.A., Makeyev,E.V. and Bamford,D.H. (2004) Initiation of viral RNA-dependent RNA polymerization. *J. Gen. Virol.*, **85**, 1077–1093.
33. Zhai,Y., Sun,F., Li,X., Pang,H., Xu,X., Bartlam,M. and Rao,Z. (2005) Insights into SARS-CoV transcription and replication from the structure of the nsp7-nsp8 hexadecamer. *Nat. Struct. Mol. Biol.*, **12**, 980–986.
34. Frick,D.N. and Richardson,C.C. (2001) DNA primases. *Annu. Rev. Biochem.*, **70**, 39–80.
35. Castro,C., Smidansky,E., Maksimchuk,K.R., Arnold,J.J., Korneeva,V.S., Götte,M., Konigsberg,W. and Cameron,C.E. (2007) Two proton transfers in the transition state for nucleotidyl transfer catalyzed by RNA- and DNA-dependent RNA and DNA polymerases. *Proc. Natl Acad. Sci. USA*, **104**, 4267–4272.
36. Yang,W., Lee,J.Y. and Nowotny,M. (2006) Making and breaking nucleic acids: two-Mg2+-ion catalysis and substrate specificity. *Mol. Cell*, **22**, 5–13.

37. Beerens,N., Selisko,B., Ricagno,S., Imbert,I., van der Zanden,L., Snijder,E.J. and Canard,B. (2007) De novo initiation of RNA synthesis by the arterivirus RNA-dependent RNA polymerase. *J. Virol.*, **81**, 8384–8395.
38. Jablonski,S.A. and Morrow,C.D. (1995) Mutation of the aspartic acid residues of the GDD sequence motif of poliovirus RNA-dependent RNA polymerase results in enzymes with altered metal ion requirements for activity. *J. Virol.*, **69**, 1532–1539.
39. Vazquez,A.L., Alonso,J.M.M. and Parra,F. (2000) Mutation analysis of the GDD sequence motif of a calicivirus RNA-dependent RNA polymerase. *J. Virol.*, **74**, 3888–3891.
40. Arnold,J.J., Ghosh,S.K. and Cameron,C.E. (1999) Poliovirus RNA-dependent RNA polymerase (3Dpol). Divalent cation modulation of primer, template and nucleotide selection. *J. Biol. Chem.*, **274**, 37060–37069.
41. Deng,T., Sharps,J., Fodor,E. and Brownlee,G.G. (2005) In vitro assembly of PB2 with a PB1-PA dimer supports a new model of assembly of influenza A virus polymerase subunits into a functional trimeric complex. *J. Virol.*, **79**, 8669–8674.
42. Luo,G., Hamatake,R.K., Mathis,D.M., Racela,J., Rigat,K.L., Lemm,J. and Colonno,R.J. (2000) De novo initiation of RNA synthesis by the RNA-dependent RNA polymerase (NS5B) of hepatitis C virus. *J. Virol.*, **74**, 851–863.
43. Arnold,J.J. and Cameron,C.E. (1999) Poliovirus RNA-dependent RNA polymerase (3Dpol) is sufficient for template switching in vitro. *J. Biol. Chem.*, **274**, 2706–2716.
44. Deming,D.J., Graham,R.L., Denison,M.R. and Baric,R.S. (2007) Processing of open reading frame 1a replicase proteins nsp7 to nsp10 in murine hepatitis virus strain A59 replication. *J. Virol.*, **81**, 10280–10291.
45. Beckman,M.T.L. and Kirkegaard,K. (1998) Site size of cooperative single-stranded RNA binding by poliovirus RNA-dependent RNA polymerase. *J. Biol. Chem.*, **273**, 6724–6730.
46. Liu,Z., Robida,J.M., Chinnaswamy,S., Yi,G., Robotham,J.M., Nelson,H.B., Irsigler,A., Kao,C.C. and Tang,H. (2009) Mutations in the hepatitis C virus polymerase that increase RNA binding can confer resistance to cyclosporine A. *Hepatology*, **50**, 25–33.
47. Yap,T.L., Xu,T., Chen,Y.-L., Malet,H., Egloff,M.-P., Canard,B., Vasudevan,S.G. and Lescar,J. (2007) Crystal structure of the dengue virus RNA-dependent RNA polymerase catalytic domain at 1.85-angstrom resolution. *J. Virol.*, **81**, 4753–4765.
48. McDonald,S.M., Aguayo,D., Gonzalez-Nilo,F.D. and Patton,T. (2009) Shared and group-specific features of the rotavirus RNA polymerase reveal potential determinants of gene reassortment restriction. *J. Virol*, **83**, 6135–6148.
49. Imbert,I., Snijder,E.J., Dimitrova,M., Guillemot,J.-C., Lécine,P. and Canard,B. (2008) The SARS-Coronavirus PLnc domain of nsp3 as a replication/transcription scaffolding protein. *Virus Res.*, **133**, 136–148.
50. Pan,J.A., Peng,X., Gao,Y., Li,Z., Lu,X., Chen,Y., Ishaq,M., Liu,D., DeDiego,M.L., Enjuanes,L. *et al.* (2008) Genome-wide analysis of protein–protein interactions and involvement of viral proteins in SARS-CoV replication. *PLoS ONE*, **3**, e3299.
51. van Hemert,M.J., van den Worm,S.H.E., Knoops,K., Mommaas,A.M., Gorbalenya,A.E. and Snijder,E.J. (2008) SARS-Coronavirus replication/transcription complexes are membrane-protected and need a host factor for activity in vitro. *PLoS Pathog.*, **4**, e1000054.
52. Labonte,P., Axelrod,V., Agarwal,A., Aulabaugh,A., Amin,A. and Mak,P. (2002) Modulation of hepatitis C virus RNA-dependent RNA polymerase activity by structure-based site-directed mutagenesis. *J. Biol. Chem*, **277**, 38838–38846.
53. Ivanov,K.A., Thiel,V., Dobbe,J.C., van der Meer,Y., Snijder,E.J. and Ziebuhr,J. (2004) Multiple enzymatic activities associated with severe acute respiratory syndrome coronavirus helicase. *J. Virol.*, **78**, 5619–5632.